$$v_n \sim \frac{AC}{\Delta t} = \frac{AB \cos \phi}{\Delta t} = -\frac{\partial h}{\partial t} \cos \phi \qquad [A-4]$$

From Eq. [A-1]-[A-4], we may finally deduce

$$\frac{\partial h}{\partial t} = -\sigma_e \left(\frac{\partial c}{\partial y} - \frac{\partial c}{\partial x} \frac{\partial h}{\partial x} \right) \quad \text{at} \quad y = h(x, t) \qquad [A-5]$$

as the moving boundary condition in two dimensions.

Considering the problem in three dimensions, *i.e.*, assuming $y = h(x, z, t)$, where z is the coordinate normal to both x and y, we may derive similarly

$$\frac{\partial h}{\partial t} = -\sigma_e \left(\frac{\partial c}{\partial y} - \frac{\partial c}{\partial x} \frac{\partial h}{\partial x} - \frac{\partial c}{\partial z} \frac{\partial h}{\partial z} \right) \quad \text{at} \quad y = h(x, z, t) \qquad [A-6]$$

REFERENCES

1. D. W. Shaw, *J. Cryst. Growth*, **47,** 509 (1979).
2. D. W. Shaw, *This Journal*, **128,** 874 (1981).
3. H. K. Kuiken, *Proc. R. Soc., London, Ser. A.*, **392,** 199 (1984).
4. H. K. Kuiken, *ibid.*, **396,** 95 (1984).
5. C. Vuik and C. Cuvelier, *J. Comp. Phys.* (1985).
6. D. W. Shaw, *This Journal*, **113,** 958 (1966).
7. W. G. Oldham and R. Holmstein, *ibid.*, **114,** 381 (1967).
8. E. Kohn, *ibid.*, **127,** 505 (1980).
9. P. H. L. Notten, J. J. Kelly, and H. K. Kuiken, *ibid.*, **133,** 1226 (1986).
10. H. Gerischer and W. Mindt, *Electrochim. Acta*, **13,** 1329 (1968).
11. H. Gerischer and I. Wallem-Mattes, *Z. Phys. Chem., N.F.*, **64,** 187 (1969).
12. P. H. L. Notten, *This Journal*, **131,** 2641 (1984).
13. E. Haroutounian, J.-P. Sandino, P. Cléchet, D. Lamouche, and J.-R. Martin, *ibid.*, **131,** 27 (1984).
14. J. O'M. Bockris and D. M. Drazic, "Electro-Chemical Science," Chap. 4, Taylor & Francis, London (1972).
15. J. R. Ockendon and W. R. Hodgkins, "Moving Boundary Problems in Heat Flow and Diffusion," p. 120, Clarendon, Oxford (1975).
16. J. Crank, "Free and Moving Boundary Problems," p. 1, Clarendon, Oxford (1984).
17. D. D. MacDonald, "Transient Techniques in Electrochemistry," Chap. 4.3, Plenum Press, New York (1977).
18. K. B. Oldham, *J. Electroanal. Chem.*, **122,** 1 (1981).
19. M. Abramowitz and I. A. Stegun, "Handbook of Mathematical Functions," p. 374, Dover, New York (1965).
20. J. R. Selman and J. Newman, *This Journal*, **118,** 1070 (1971).
21. W. van Erk and H. K. Kuiken, *J. Cryst. Growth*, **51,** 397 (1981).
22. H. K. Kuiken and R. P. Tijburg, *This Journal*, **130,** 1722 (1983).
23. V. G. Levich, "Physicochemical Hydrodynamics," Chap. 2, Prentice Hall, Englewood Cliffs, NJ (1962).
24. R. B. Bird, W. E. Stewart, and E. N. Lightfoot, "Transport Phenomena," John Wiley and Sons, New York (1960).
25. S. G. Springer and T. J. Pedley, *Proc. R. Soc., London, Ser. A*, **333,** 347 (1973).
26. H. Gerischer, *Ber. Bunsenges. Phys. Chem.*, **69,** 578 (1965).
27. W. Kern, *R.C.A. Rev.*, **39,** 278 (1978).
28. G. Gerlagh and P. Baeyens, *Trans. Inst. Met. Finishing*, **53,** 133 (1975).
29. W. Kern, in "Etching for Pattern Definition," H. G. Hughes and M. J. Rand, Editors, p. 1, The Electrochemical Society Softbound Proceedings Series, Princeton, NJ (1976).

Etching Profiles at Resist Edges

II. Experimental Confirmation of Models Using GaAs

P. H. L. Notten, J. J. Kelly, and H. K. Kuiken

Philips Research Laboratories, 5600 JA Eindhoven, The Netherlands

ABSTRACT

Etching experiments have been carried out with GaAs in order to check mathematical models developed for diffusion-controlled dissolution at resist edges. Both electroless and chemical etchants were used, and their chemistry is briefly considered. An interesting method of controlling the electroless dissolution rate of GaAs by means of a diffusion-controlled oxidation reaction is reported. The excellent agreement between calculated and measured etched profiles demonstrates the validity of the mathematical model. The influence of natural convection and of convection induced by gas evolution is reported, and the results are compared with theory.

In Part I (1) a mathematical model was presented to describe diffusion-controlled etching at resist edges. Both the form of the etched profiles and the characteristics of the etching kinetics at the edges are predicted by the model.

In the present paper we attempt to verify the model experimentally. In order to do this, we need etching systems that meet two main requirements (1). (*i*) The etch rate on all crystal planes of the solid must be determined by mass-transport in the solution, *i.e.*, the rate constant for the rate-determining step of the dissolution process must be sufficiently large to ensure a very low surface concentration of the rate-determining species, even at the slowest etching plane. (*ii*) The dimensionless etching parameter β, introduced in Part I to describe the dissolution process, must be large (≥ 100).

Etching methods not involving an external current or voltage source can be divided into two classes: electroless and chemical (2). Electroless etching occurs at a well-defined mixed potential that is determined by two potential-dependent electrochemical reactions; at this potential, the rates of dissolution of the solid and reduction of the oxidizing agent in the solution are equal. Chemical dissolution is observed with bifunctional molecules that are capable of forming new bonds with two neighboring surface atoms simultaneously. The etch rate, in this case, does not depend on the surface concentration of charge carriers in the solid and is not influenced by an externally applied potential (3).

As a model system in the present work, the etching of GaAs, which is very important for device applications, was considered. This material can be dissolved with both electroless and chemical etchants. In order to decide on how to comply with the requirements of the mathematical model, we examined the chemistry of possible etching systems. Apart from the two requirements described above, the precise etching mechanism is important in determining the etched profiles. For this reason, we first consider briefly the mechanism of electroless and chemical dissolution of GaAs. Results obtained experimentally with suitable etchants are then described and compared with those predicted by theory.

Choice of Etchants for GaAs

Electroless dissolution.—Electroless etching consists of two electrochemical partial reactions: oxidative dissolution of the solid and reduction of an oxidizing agent from solution (2). A simple representation of the oxidation reaction can be given as follows (3)

$$\text{Ga:As} + h^+ + X^- \xrightarrow{k'_a} \text{Ga}\cdot\text{As}(X) \quad [1]$$

$$\text{Ga}\cdot\text{As}(X) + h^+ + X^- \xrightarrow{k''_a} \text{Ga As}(X,X) \xrightarrow[4h^+]{\text{fast}} \text{Ga}^{III} + \text{As}^{III} \quad [2]$$

Valence band holes h^+ are trapped in Ga-As surface bonds and attack by a nucleophilic species X^- (*e.g.*, OH^- ions) from solution results in the formation of new Ga-*X* and As-*X* bonds. Hole trapping and nucleophilic attack can also occur in consecutive reactions. However, the precise mechanism is not important here. In total, 6 charge carriers are required to dissolve one GaAs entity and trivalent species are formed in solution (reaction [2]). If the various steps in the above reaction scheme are irreversible, then the current due to the total oxidation reaction i_a is given by

$$i_a = 6\mathbf{F}k'_a p_s C_X^0 \quad [3]$$

where p_s, the surface hole concentration, is an exponential function of applied potential, C_X^0 is the surface concentration of the nucleophilic reagent, k'_a is the rate constant of the first step, and **F** is the Faraday constant.

In an electroless system, the holes required for oxidative dissolution must be injected from the oxidizing agent (4, 5)

$$\text{Ox}^{n+} \xrightarrow{k_c} \text{Red} + n\cdot h^+ \quad [4]$$

The corresponding reduction current is given by

$$i_c = n\mathbf{F}k_c C_{ox}^0 \quad [5]$$

where C_{ox}^0 is the surface concentration of the oxidizing agent. During electroless etching, oxidation and reduction reactions occur simultaneously, and the partial currents must be equal ($i_a = i_c$). For example, in the case of a $Fe(CN)_6^{3-}$ etchant, the total reaction is

$$\text{GaAs} + 6\text{Fe(CN)}_6^{3-} \rightarrow \text{Ga}^{III} + \text{As}^{III} + 6\text{Fe(CN)}_6^{4-} \quad [6]$$

On the basis of Eq. [1]-[5] and the values of the rate constants for the anodic and cathodic processes, it is clear that diffusion-controlled etching might be achieved in two ways. (*i*) The most common case, that shown for p-GaAs in Fig. 1, involves a redox system with a very large value of k_c. The surface concentration of the oxidizing agent is then very small, and reduction is limited by its mass transport in solution. The diffusion current (curve (a), Fig. 1) is directly proportional to the concentration of the oxidizing agent. When a rotating disk electrode (RDE) is used (6), this current is proportional to the square root of the rotation rate (insert, Fig. 1). The oxidation reaction is kinetically controlled; $k'_a \cdot p_s$ is sufficiently small so that X^- is not depleted at the electrode surface. The anodic current depends exponentially on the potential (curve (b)). The total current, which is that actually measured, is the sum of the partial currents (curve (c)). At the rest or open-circuit potential V_r, the partial currents are equal. The etch rate, which can be calculated from the partial current, is obviously determined by diffusion-controlled reduction of the oxidizing agent. (*ii*) If $k'_a \cdot p_s$ in Eq. [3] is relatively large and the concentration of X^- is limited, it might be expected that anodic dissolution becomes diffusion controlled. We have shown this to be clearly the case for electrolytes with a pH in the range 11-14. Figure 2 gives the current-potential curve for anodic dissolution of a p-type GaAs RDE in NaOH solution of pH = 12. The current first increases exponentially but becomes constant at more positive potentials. This limiting current depends on the square root of the rotation rate (see insert of Fig. 2); it is clearly determined by mass transport of a species in solution. A plot of the log of the current density *vs.* pH gives a straight line of unit slope (Fig. 3); it follows that OH^- must be the rate-determining species.

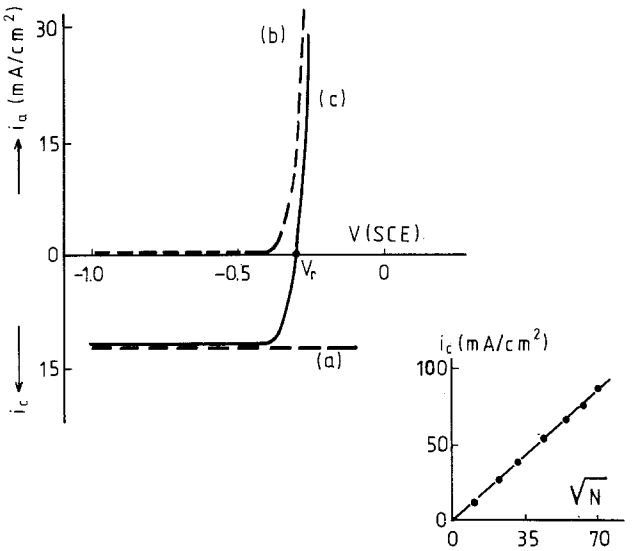

Fig. 1. Current-potential curves for a p-type GaAs RDE in a 0.1M $K_3Fe(CN)_6$ solution at pH = 14 (electrode rotation rate N = 100 rpm). Curves (a) and (b) refer to the cathodic and anodic partial reactions, respectively. Curve (c) is the total measured curve. V_r is the rest potential. The dependence of the cathodic limiting current on rotation rate is given in the insert.

If such an anodic process is combined with a cathodic reaction, which is not rate limiting, then the rate of electroless etching at the rest potential must be determined by the diffusion-controlled anodic reaction. This case is illustrated for $Fe(CN)_6^{3-}$ solution at pH = 12 in Fig. 4. The measured etch rate agrees with that calculated on the basis of the anodic limiting current. It depends on the rotation rate and the OH^- concentration but is independent of the $Fe(CN)_6^{3-}$ concentration.

For electroless etching of n-type III-V materials, the form of the partial current-potential curves is somewhat different (4, 5), because the oxidizing agent now injects minority carriers (holes) into the valence band of the solid. However, the electroless etching kinetics of n-type and p-type samples of a given material in these etchants are the same (4, 5).

Chemical dissolution.—In order to introduce the mathematical model in Part I, the chemical etching of GaAs was

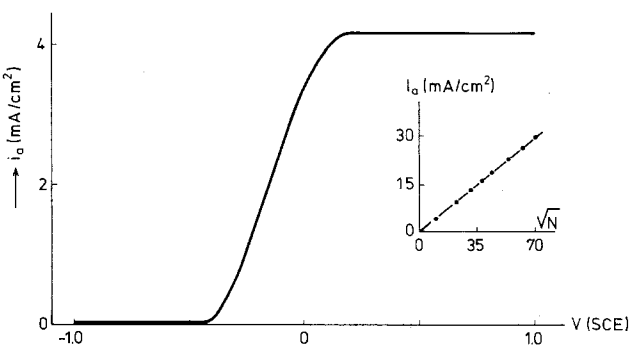

Fig. 2. The anodic current-potential curve for a p-type GaAs RDE in an NaOH solution, pH = 12 (N = 100 rpm). The dependence of the anodic limiting current on rotation rate N is shown in the insert.

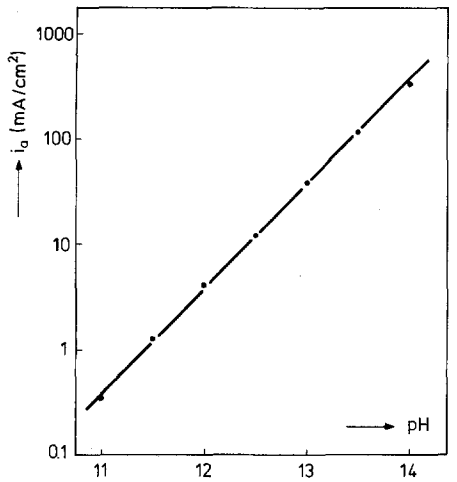

Fig. 3. The dependence of the anodic limiting current of a p-type GaAs RDE, measured at 100 rpm, on the pH of the NaOH electrolyte.

described in general terms. Here, we shall confine ourselves to a brief consideration of one of the systems used in the present work: $HCl/H_2O_2/H_2O$ etchants. GaAs does not dissolve in concentrated HCl solutions. Addition of the oxidizing agent H_2O_2 to HCl yields suitable etchants (7). The etching mechanism is, however, different from that described in the previous section. This is clear from the current-potential curve [curve (a)] shown in Fig. 5 for a p-type GaAs electrode in an $HCl/H_2O_2/H_2O$ solution. As previously found, H_2O_2 is not reduced cathodically at a significant rate on p-type GaAs in the dark (8). The cathodic current required to account for the measured etch rate, assuming an electroless mechanism of the type described above, is shown in Fig. 5 by the dashed line (b).

We conclude that dissolution occurs via a purely chemical mechanism, which does not involve mobile charge carriers in the semiconductor and is not influenced by the applied potential (2, 3)

$$\text{Ga—As} + H_2O_2 \xrightarrow{k_s} \begin{matrix}\text{OH} & \text{OH}\\ | & |\\ \text{Ga} & \text{As}\end{matrix} \qquad [7]$$

$$\begin{matrix}\text{OH} & \text{OH}\\ | & |\\ \text{Ga} & \text{As}\end{matrix} \xrightarrow[H_2O_2,\ HCl]{\text{fast}} Ga^{III} + As^{III} \qquad [8]$$

A coordinated reaction sequence occurs involving the rupture of Ga-As and HO-OH bonds and the simultaneous formation of new Ga-OH and As-OH bonds. If reaction [7] is rate determining and its rate constant k_s is large, then etching is diffusion controlled and determined by the H_2O_2 concentration in solution. We found this to be the case at large values of the concentration ratio $[HCl]/[H_2O_2]$. Since this holds for all crystal faces of GaAs, such etchants are suitable in the present investigation.

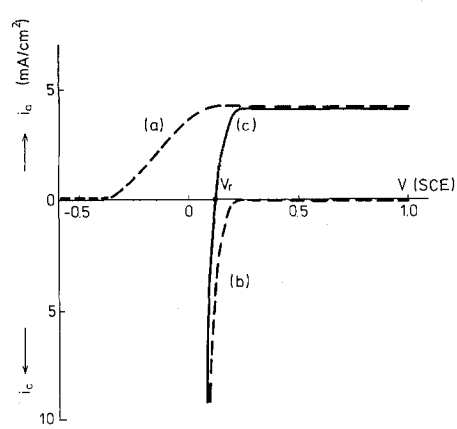

Fig. 4. Current-potential curves for a p-type GaAs RDE in a 0.5M $K_3Fe(CN)_6$ solution at pH = 12 (N = 100 rpm). Curves (a) and (b) refer to the anodic and cathodic partial reactions, respectively. Curve (c) is the total measured curve. V_r is the rest potential of the electrode.

In this type of etchant, HCl may be replaced by other (nonoxidizing) acids such as H_3PO_4 (9) and H_2SO_4 (10). Again, the concentration ratio of acid to H_2O_2 determines the etching kinetics. At large values of this ratio, etching is, under normal conditions, dependent on H_2O_2 diffusion for all planes of GaAs except the (111)-Ga plane (9, 10). Since etching of the Ga surface remains kinetically controlled, etchants based on H_2SO_4 and H_3PO_4 have not been used in the present work.

The dimensionless parameter β.—Once the etching mechanism has been established by kinetic and electrochemical measurements and the rate-determining species has been identified, the value of the dimensionless etching parameter β can be calculated

$$\beta = \frac{m\rho_s}{CM_s} \qquad [9]$$

For our model to be valid, a large value of this parameter is essential (1). For a given solid, the density ρ_s and molecular weight M_s are fixed. The number of ions or molecules m of the rate-determining species required to dissolve one atom or molecule of the solid is determined by the etching process. The concentration of the rate-determining species C can be used to adjust the β value. As shown in Table I of the previous paper (1), the etchants used in this study comply with the β requirement of the model.

Experimental

The n-type and p-type GaAs slices, with (100) orientation and a carrier density of approximately $10^{18}/cm^3$, were obtained from MCP Electronics, Limited. The samples were mechano-chemically polished before use.

The etchants used are listed in Table I. Both H_2O_2 (30% solution) and HCl (37% solution) were of Selectipur quality supplied by Merck. NaOCl was obtained as an approximately 1M solution in 0.1M NaOH from BDH Chemicals, Limited. All other chemicals were obtained from Merck and were of p.a. grade. Etching was performed at room temperature. In Table I, we also specify the etching mode (electroless or chemical) and the determining species in solution. It should be noted that solutions of HCl with very strong oxidizing agents (H_2O_2 and NaOCl) are inherently unstable, since chloride can be oxidized to chlorine. Gas evolution in $HCl/H_2O_2/H_2O$ etchants begins rather slowly, and a slight yellowish coloration of the solution indicates some Cl_2 formation. However, the rate of this reaction is limited, and H_2O_2 is the active component of the etching bath. Etching was performed, in this case, immediately after the solution components were mixed. When hypochlorite and HCl are mixed, a very vigorous Cl_2 evolution is immediately observed. This subsides after some minutes. The etching experiments with this bath were performed 3 min after mixing when only a very slight gas evolution occurred. Since electrochemical measurements, similar to those given in Fig. 5 for the HCl/H_2O_2 system, showed that the cathodic current in the HCl/NaOCl solution cannot account for the measured etch rate, we conclude that this solution also etches chemically and that Cl_2 is the active component. For both H_2O_2- and NaOCl-based etchants, a fresh solution was prepared for each etching experiment.

In most cases, an SiO_2 layer was used to mask half the GaAs surface. Photoresists (HNR-999 and HPR-204 from Shipley) were also used in certain cases. The resist edge was generally parallel to the (110) direction. The samples (6 × 6 mm) were mounted on a glass plate and placed vertically in the etching solution with the resist edge parallel to the solution surface and the free GaAs surface below the masked area. After etching, we cleaved the slices perpendicular to the resist edge and examined the etched profiles in a scanning electron microscope (SEM). For

Table I. GaAs etchants

Etchant and composition	Oxidizing agent	Rate-determining Species Concentration		Etching mode
$HCl:H_2O_2:H_2O$ = 160:4:1[a]	H_2O_2	H_2O_2	0.24*M*	Chemical
= 80:4:1[a]	H_2O_2	H_2O_2	0.46*M*	Chemical
1*M* NaOCl:HCl[b] = 5:1[a]	Cl_2	Cl_2	1*M*	Chemical
1*M* NaOCl in 0.1*M* NaOH[c] 0.1*M* Na_2CO_3	OCl^-	OH^-	<0.1*M*	Electroless (Anodic control)
0.05*M* $K_3Fe(CN)_6$, pH = 13	$Fe(CN)_6^{3-}$	$Fe(CN)_6^{3-}$	0.05*M*	Electroless (Cathodic control)
0.5*M* $K_3Fe(CN)_6$, pH = 13	$Fe(CN)_6^{3-}$	OH^-	0.1*M*	Electroless (Anodic control)

[a] Volume ratio of component solutions (HCl (37%), H_2O_2 (30%), NaOCl (± 1*M* solution in 0.1*M* NaOH)).
[b] Etchant cited in Ref. (11).
[c] Etchant cited in Ref. (12).

one series of experiments, larger GaAs slices were used. Instead of masking half the surface, as described above, we left unmasked a parallel strip, 4 mm wide, between resist areas at the top and bottom of the slice (see Fig. 9). The direction of the resist edges and the method of etching were the same as for the "half-masked" slices.

When very thin resist layers were used, a slight curling of the resist at the etched edge was sometimes observed in the SEM [see for example Fig. 6 (a)]. This occurred after the sample was removed from the etchant. Somewhat thicker resist layers did not show this effect. The shape of the etched profiles was the same in all cases.

The experimental details for the electrochemical measurements, described in the previous section, were the same as those reported elsewhere (6).

Results and Discussion

Comparison of experiment and theory.—The mathematical model for mass-transport-controlled etching, as described in Part I, predicts a rounded profile with considerably enhanced etching at the resist edge. In Fig. 6 (a), a SEM photo is shown of a profile obtained in the chemical etchant $HCl/H_2O_2/H_2O$ (160/4/1). In Fig. 6 (b), the measured profile is compared with that calculated from the theoretical model. The calculated curve was fitted on one point, viz., that at which the under(etched) GaAs surface meets the resist edge. The excellent agreement between the measured and the calculated curves demonstrates clearly the validity of the mathematical treatment. It should be noted that the measured etch factor, defined by y_b/x_0 [see Fig. 6 (b)], agrees very well with the value of 1.33 predicted by theory. The right angle at which the profile meets the underside of the mask is also in full agreement with theory.

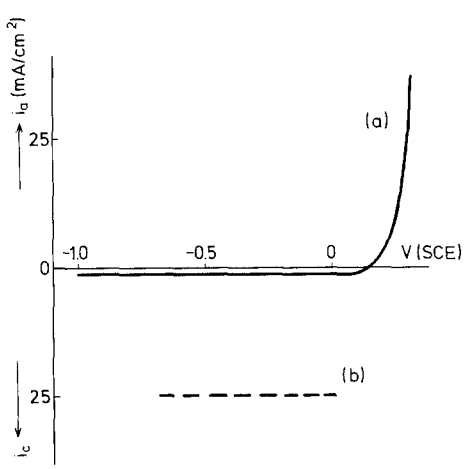

Fig. 5. Curve (a) shows the measured current-potential characteristics of a p-type GaAs electrode in a $HCl/H_2O_2/H_2O$ (160/4/1) solution (see Table I). Curve (b) shows the hypothetical cathodic current required to account for the measured etch rate at V_r, assuming an electroless mechanism.

Influence of forced convection.—Figure 7 shows the development of the etched profile as a function of time for a $HCl/H_2O_2/H_2O$ (80/4/1) solution. From the corresponding figure (Fig. 8), it is clear that, in the vicinity of the mask edge, agreement between experimental and theoretical profiles is very good. It should be emphasized that these curve fits were carried out only according to shape, not according to absolute position. Indeed, the theory presented in Part I is only complete for stationary etchants. For the results shown in Fig. 7, convection must have been an important factor. This was evident from the gas evolution observed in solution. The rate of evolution increased with time, as described in the Experimental section. However, referring to the analysis of Part I, we know that, during the initial stages of an etching process that is dominated by convection, the shape of the profile in the vicinity of the mask is still predicted quite accurately by the stationary etchant approach.

When the results of Fig. 8 are studied more closely, we see that the fit in the mask edge region is excellent for the smaller of the etched depths. However, Fig. 8 (d), which refers to a relatively large depth, shows a departure from the theoretical prediction, suggesting that convection is beginning to influence the shape of the profile. Assuming that forced convection rather than natural (solutal) convection is dominant, we may now use Eq. [66] of Part I to estimate the time t up to which convection

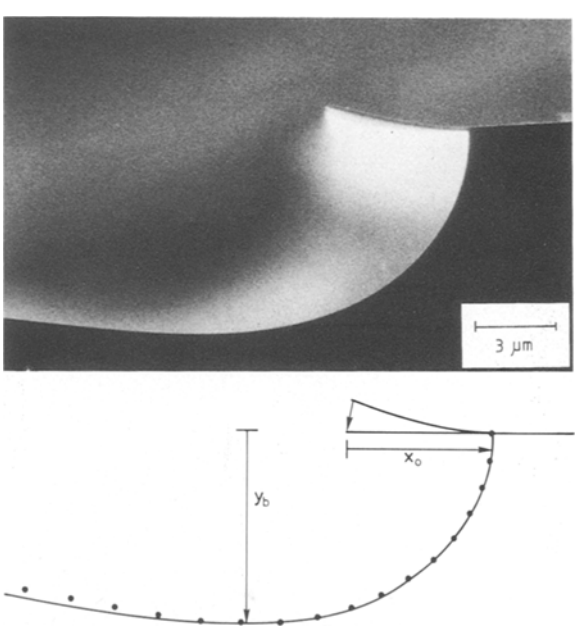

Fig. 6. (a, top) SEM photo of a profile etched in GaAs using a $HCl/H_2O_2/H_2O$ (160/4/1) solution. Etching time: 5 min. Figure 6 (b, bottom) shows the agreement between the profile measured in 6 (a) (continuous line) and that calculated from theory (filled circles). The undereteching x_0 and the maximum etched depth y_b are also shown.

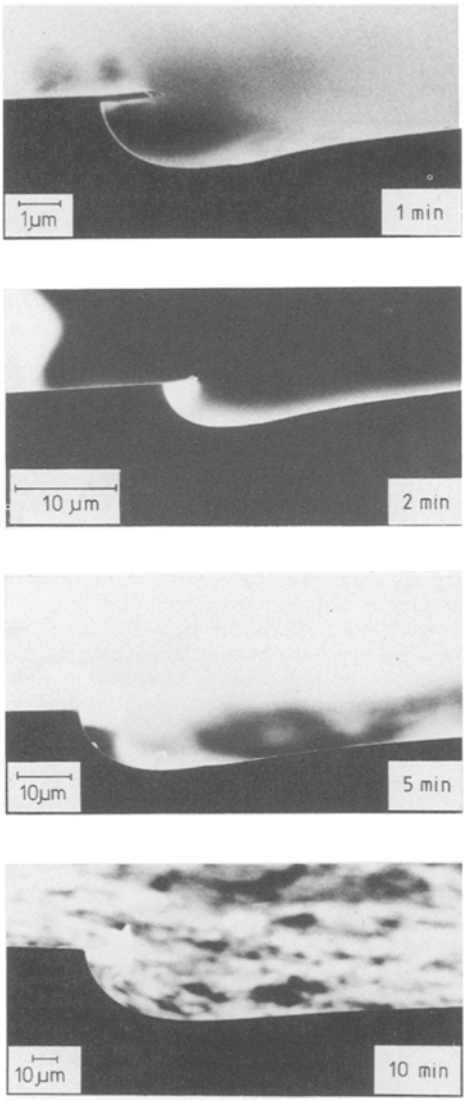

Fig. 7. The development of the etched profile with etching time for GaAs in a $HCl/H_2O_2/H_2O$ (80/4/1) solution.

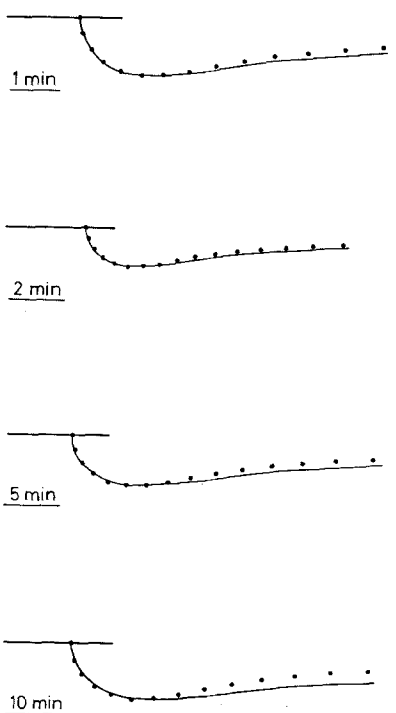

Fig. 8. Comparison of the measured (continuous curve) and calculated results (filled circles) for the etched profiles in Fig. 7.

does not markedly affect the shape of the etched profile in the corner region. From Eq. [46] and [66] of Part I we have

$$t \ll \frac{\beta \delta_u}{u_0} \qquad [10]$$

where u_0 is a measure for the average velocity of the solution in the etching vessel. Denoting the dimensions of the vessel by L, we may estimate δ_u as follows

$$\delta_u \approx L\,\mathrm{Re}^{-1/2} \qquad [11]$$

where Re is the Reynolds number

$$\mathrm{Re} = \frac{u_0 L}{\nu} \qquad [12]$$

where ν is the kinematic viscosity (m^2/s). From Eq. [10]-[12], we may deduce

$$t \ll \beta \cdot \left(\frac{L\,\nu}{u_0^3}\right)^{1/2} \qquad [13]$$

Of the parameters appearing on the right-hand side of Eq. [13], the value of u_0 is the most difficult to appraise. As described above, the etchant is stirred by moving gas bubbles. The average velocity of the etchant will depend on the relative volume occupied by these bubbles. Assuming u_0 to be 10^{-3} m/s, which is substantially lower than the velocity of the bubbles, we have from [13]

$$t \ll 1300\text{s} \qquad [14]$$

for $L \approx 0.03$m, $\nu \approx 10^{-6}$ m^2/s, and $\beta \approx 240$ (Table I of Part I). This admittedly rough analysis would seem to confirm our observation (Fig. 8 (d)) that convection is already showing its influence in the mask edge region after 10 min etching.

Using the same numerical estimates as before, we can try to assess the corresponding etched depth. With $t \approx$ 600s (Fig. 7 (d)) and an average velocity u_0 during this period of 10^{-3} m/s, we have Re $\approx$ 30. Taking $D \approx 10^{-9}$ m^2/s, we may calculate the characteristic length l ($\approx$ 74 μm) with the aid of Eq. [11] from this work and Eq. [46] from Part I. Using Eq. [67] from Part I, we then predict an etched depth of 25 μm, which compares favorably with the measured value of 26.7 μm. This merely serves to show that an average velocity of around 10^{-3} m/s was a reasonable estimate for this particular experiment.

Further away from the mask edge, theory and experiment are in less good agreement for all cases presented in Fig. 8. These differences become more pronounced at longer etching times. Two factors play a role here. The first of these is that the theoretical curve given by Fig. 9 (Part I) and Table II (Part I) refers only to the blown up region in the vicinity of the mask. Outside this region, the profile should tend to the behavior as predicted by Eq. [26] (absence of convection) or Eq. [52] (with convection). It is shown in Ref. (13) that a composite profile, constructed on the basis of these two contributions, provides a better approximation to the curve, particularly in the area just outside the mask edge region. Applying the rules given in (13), we find that the composite profile coincides reasonably with the experimental profiles of Fig. 8 (a) and 8 (b) for a β value of approximately 75. Since $\beta \approx$ 240, this does not fully explain the difference between theory and experiment. Consequently, such differences, even those of Fig. 8 (a) and 8 (b), have to be attributed mainly to convection. The much larger discrepancy shown in Fig. 8 (d) is certainly due to this effect.

"Solutal" convection.—Another experimental result that shows a strong influence of convection is presented in Fig. 9. These two photographs refer to etching of a GaAs strip between masked areas. As in the previous cases, the substrate was kept in a vertical position with the mask edges parallel to the solution surface. Figure 9 (a) shows the profile near the upper mask edge and 9 (b) that near the lower mask edge, etched at the same time. Clearly,

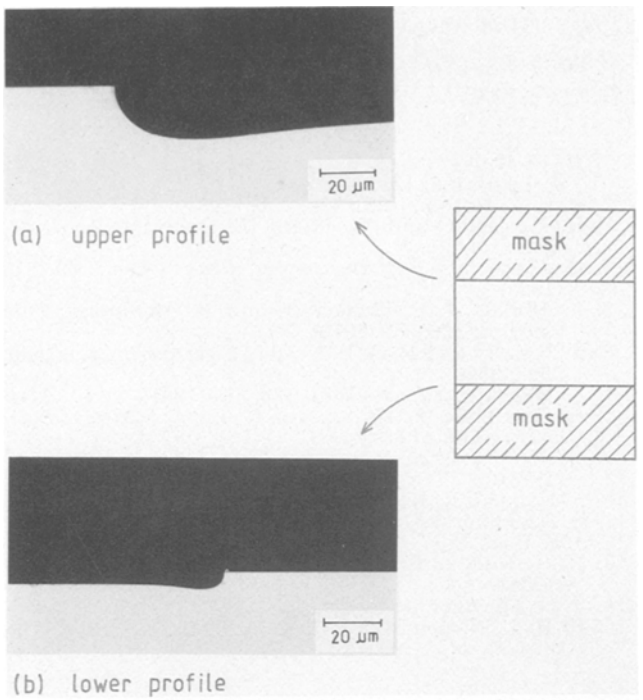

Fig. 9. The effect of "solutal" convection on GaAs etching in a 0.5M $K_3Fe(CN)_6$ solution at pH = 13. Figure 9 (a) shows the profile obtained at the top edge of the resist/unmasked GaAs strip. Figure 9 (b) was observed at the lower GaAs/resist edge. The sample geometry, as shown in the insert, is described in the text.

these etched depths are different. In this experiment, we used a 0.5*M* $Fe(CN)_6^{3-}$ solution at pH = 13, which did not produce gas bubbles. As a result, forced convection is not expected to be a dominant factor here.

The explanation for the different etch rates observed in Fig. 9 is to be found in the phenomenon of solutal convection, which is caused by density gradients due to spatial variation of the composition of the etchant. Figure 9 reveals that this solutal flow must have been directed downwards. The shape of Fig. 9 (a) can again be explained along the lines laid down in Part I. For the explanation of the profile in Fig. 9 (b), we may refer to Ref. (14). That paper considers heat transfer near the trailing edge (as defined by the flow direction) of a hot surface. Since our simple mass-transfer model is mathematically equivalent to the corresponding heat-transfer model, we may use the results of this publication here. In Ref. (14), it is shown that the heat-transfer function $q(\overline{X})$ (see Eq. [52] and [53] of Part I) becomes singular not only near $\overline{X} = 0$, but also near the trailing edge of the heated region. Moreover, this is again an inverse square root singularity, as in Eq. [55] of Part I. However, the coefficient of this singularity is smaller than the factor 0.44 reported there. Its value depends on the width of the nonmasked area. Referring to our analysis of Part I, we may again expect that, in the case of etching, this singularity will result in a local bulging shape of the profile. Since the coefficient of the singularity is smaller, the ensuing bulge should be less pronounced.

Another way of looking at this is that, as the boundary layer develops along the unmasked surface in a downward direction, the etchant is gradually depleted. The etched depth is almost proportional to the local mass-transfer function (see Eq. [52] of Part I), which slowly tends to zero in the downward direction (increasing $\overline{X}$). When the results of Fig. 9 are studied more closely away from the mask edge region, it is seen that the variation of the etched depth with distance in Fig. 9 (a) is more pronounced (also in a relative sense) than in Fig. 9 (b). Indeed, in Fig. 9 (b), the profile is almost flat just outside the bulging region. This shows that $q(\overline{X})$ varies more slowly as $\overline{X}$ increases.

Etch rates.—According to the theory of Part I, the time dependence of the etched depth depends markedly on the hydrodynamics of the etching process. For a purely diffusion-controlled reaction, the etch depth at the deepest point y_b should depend on the square root of the etching time (Eq. [39], Part I). As discussed in Part I, this case is rarely encountered in etching systems, since convection always plays a role in mass transport. This observation has already been corroborated by the experimental evidence we have discussed above.

If convective diffusion is considered with a linearized and stationary velocity assumption (1), then a $t^{2/3}$ dependence is expected for etching in the mask edge region (Eq. [67], Part I). Figure 10 shows a plot of the etched depth at the deepest point as a function of etching time for three different systems. For curve (a) measured with the NaOCl etchant of pH = 13, which operates without gas evolution, the slope 0.6 suggests a case intermediate between the two cases discussed above. The HCl/NaOCl etchant [curve (b)] gives a slope of 0.78, which is reasonably close to that expected for the convective-diffusion model. The etchant produces very little gas during the experiments. The third solution ($HCl/H_2O_2/H_2O$) shows a

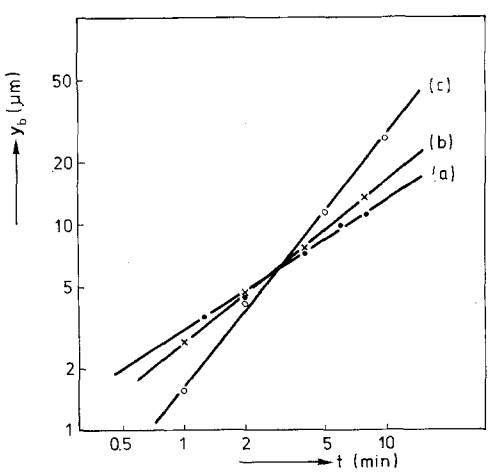

Fig. 10. The etched depth y_b at the deepest point of the profile as a function of etching time for 3 different etchants: (a) 1M NaOCl, 0.1M Na_2CO_3 in 0.1M NaOH; (b) 1M NaOCl/HCl (5/1); (c) $HCl/H_2O_2/H_2O$ (80/4/1).

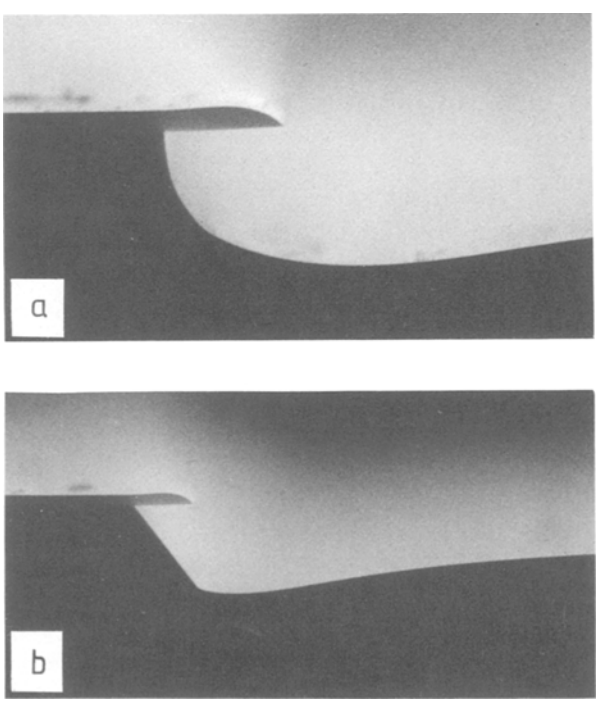

Fig. 11. Profiles obtained with electroless etchants: (a) 1M NaOCl, 0.1M Na_2CO_3 in 0.1M NaOH; (b) 0.05M $K_3Fe(CN)_6$ solution, pH = 13.

much stronger time dependence (the slope of curve (c) is 1.27). This is clearly due to forced convection, which results from gas evolution during etching; the rate of evolution increases with etching time.

Electroless etching.—An apparent anomaly was observed in the results with electroless etching systems. For those etchants in which the dissolution rate was determined by the anodic partial reaction (*i.e.*, by diffusion of OH^- ions, as in Fig. 4) the etched profile [Fig. 9 (a) and 11 (a)] was identical to that observed for the chemical etchants described above. For etchants that were "cathodically controlled" (see Fig. 1), rounded profiles were not found, despite the fact that the macroscopic etch rate of all crystal faces was shown to be diffusion controlled. Instead, the typical (111) Ga surface was exposed during dissolution [Fig. 11 (b)]. This phenomenon, which results from a characteristic electrochemical interaction between different crystal faces during etching, will be discussed in a future paper (15).

Acknowledgment

The authors wish to thank C. J. Geenen for performing the SEM measurements and J. E. A. M. van den Meerakker for helpful discussions.

Manuscript received April 22, 1985.

Philips Research Laboratories assisted in meeting the publication costs of this article.

REFERENCES

1. H. K. Kuiken, J. J. Kelly, and P. H. L. Notten, *This Journal*, **133**, 1217 (1986).
2. P. H. L. Notten, *ibid.*, **131**, 2641 (1984).
3. H. Gerischer and W. Mindt, *Electrochim. Acta*, **13**, 1329 (1968).
4. H. Gerischer, *Ber. Bunsenges. Phys. Chem.*, **69**, 578 (1965).
5. L. Hollan, J. C. Tranchart, and R. Memming, *This Journal*, **126**, 855 (1979).
6. J. J. Kelly and P. H. L. Notten, *Electrochim. Acta*, **29**, 589 (1984).
7. D. W. Shaw, *This Journal*, **128**, 874 (1981).
8. H. Gerischer, N. Müller, and O. Haas, *J. Electroanal. Chem.*, **119**, 41 (1981).
9. Y. Mori and N. Watanabe, *This Journal*, **125**, 1510 (1978).
10. S. Iida and K. Ito, *ibid.*, **118**, 768 (1971).
11. S. Adachi and K. Oe, *ibid.*, **130**, 2427 (1983).
12. J. S. Basi, U.S. Pat. 3,738,882.
13. H. K. Kuiken, *Proc. R. Soc., London, Ser. A*, **392**, 199 (1984).
14. S. G. Springer, *ibid.*, **337**, 395 (1974).
15. P. H. L. Notten and J. J. Kelly, *This Journal*, To be published.

Low Temperature Silicon Epitaxy by Hot Wall Ultrahigh Vacuum/Low Pressure Chemical Vapor Deposition Techniques: Surface Optimization

B. S. Meyerson,* E. Ganin, D. A. Smith, and T. N. Nguyen

IBM, T. J. Watson Research Center, Yorktown Heights, New York 10598

ABSTRACT

Fundamental equilibrium considerations derived from the $Si/H_2O/O_2/SiO_2$ system have been successfully employed in the design and operation of a novel low temperature epitaxial silicon process. Films have been deposited in the range $750° < T < 850°C$, with all resulting material epitaxial. TEM studies showed the transition to high quality, low defect density material to occur between 750° and 800°C, and such films were found to be of high chemical purity as well. In addition, UHV/CVD is shown to be a high throughput multiwafer system, achieving good film uniformities in a high wafer packing density environment, attributable to operation in the low pressure limit of chemical kinetics.

Over the past decade, the deposition of homoepitaxial silicon films for technological applications has been performed in essentially the same manner. Typically, this operation takes place at temperatures in excess of 1000°C, using a cold wall/hot susceptor deposition apparatus (1). Although advances in the technique with respect to the reduction of autodoping (2) by a lowering of processing pressures have allowed its continued use, a new generation of Si epitaxial growth techniques will be required to fabricate future devices which call for abrupt transitions in dopant concentration between adjacent single crystal layers. The common feature of such new deposition techniques will of necessity be low process temperatures, and there are several classes of such techniques being developed (3). We report in the following text the development, from first principles, of a UHV/CVD technique, which exploits basic chemical equilibria data (4, 5) for the $Si/O_2/H_2O/SiO_2$ system in its design and operating criteria.

The crystallographic perfection of the initial Si surface upon which epitaxy is to take place is the determining factor in the quality of the resultant epitaxial layer. Systematic investigations (6) have been done to delineate the optimum cleaning procedures for a silicon surface prior to its insertion into a deposition apparatus. However, the quality of the environment into which one is introducing this clean Si is frequently ignored. Basic surface investigations of the $Si/O_2/H_2O/SiO_2$ equilibrium system by Ghiddini and Smith (4, 5) have been employed here to establish quantitative criteria for the processing environment, where both oxygen and water vapor background in the system are such that silicon is effectively etched by those species (net reactions [1] and [2])

$$Si(s) + O_2 \rightarrow 2SiO(g) \quad [1]$$

$$Si(s) + H_2O \rightarrow SiO(g) + H_2(g) \quad [2]$$

thus favoring the maintenance of an oxide-free silicon surface. Extrapolating their data for water vapor downward in temperature (Fig. 1), it can be estimated that one must maintain a partial pressure of less than 10^{-8} torr H_2O in order to achieve an oxide free surface at 800°C. Data for oxygen showed a somewhat less severe requirement, $\sim 10^{-7}$ torr at 800°C. Using these figures as minimum design criteria, the UHV/CVD system described below was designed and assembled. Furthermore, system operating conditions were chosen using the criteria for the maintenance of an oxide free surface as a guide. An example of what is meant is as follows.

Assuming one employs conventional RPCVD (reduced pressure CVD) epitaxial silicon processing, typical process pressures are in the 10-100 torr range. Hydrogen carrier gas used in such a process at best remains pure to 1 ppm H_2O when it reaches the process environment. Thus,

*Electrochemical Society Active Member.